NANO LETTERS

Letter

pubs.acs.org/NanoLett

Cell-Penetrating Nanobiosensors for Pointillistic Intracellular Ca^{2+}-Transient Detection

Alsu I. Zamaleeva,[†,‡,§] Mayeul Collot,[∥,⊥,¶] Eloi Bahembera,[○,●] Céline Tisseyre,[○,●] Philippe Rostaing,[†,‡,§] Aleksey V. Yakovlev,[†,‡,§] Martin Oheim,[□,■] Michel de Waard,[○,●] Jean-Maurice Mallet,[∥,⊥,¶] and Anne Feltz*[,†,‡,§]

[†]Ecole Normale Supérieure, Institut de Biologie de l'ENS (IBENS), Paris F-75005, France

[‡]INSERM U1024, Paris F-75005, France

[§]CNRS UMR 8197, Paris F-75005, France

[∥]UPMC Université Paris 06, Ecole Normale Supérieure (ENS), Paris, F-75005 France

[⊥]CNRS UMR 7203, Paris F-75005, France

[¶]Laboratory of Biomolecules (LBM), Paris F-75005, France

[□]Brain Physiology Laboratory, Université Paris Descartes, PRES Sorbonne Paris Cité, Paris F-75006, France

[■]CNRS UMR 8118, Paris F-75006, France

[○]Inserm U836, Grenoble Neuroscience Institute, Research Group 3, LabEx Ion Channel Science and Therapeutics, BP170, 38042 Grenoble Cedex 09, France

[●]Université Joseph Fourier, Grenoble, France

Supporting Information

ABSTRACT: Small-molecule chemical calcium (Ca^{2+}) indicators are invaluable tools for studying intracellular signaling pathways but have severe shortcomings for detecting local Ca^{2+} entry. Nanobiosensors incorporating functionalized quantum dots (QDs) have emerged as promising alternatives but their intracellular use remains a major challenge. We designed cell-penetrating FRET-based Ca^{2+} nanobiosensors for the detection of local Ca^{2+} concentration transients, using commercially available CANdot565QD as a donor and CaRuby, a custom red-emitting Ca^{2+} indicator, as an acceptor. With Ca^{2+}-binding affinities covering the range of 3−20 μM, our CaRubies allow building sensors with a scalable affinity for detecting intracellular Ca^{2+} transients at various concentrations. To facilitate their cytoplasmic delivery, QDs were further functionalized with a small cell-penetrating peptide (CPP) derived from hadrucalcin (Had_{UF1-11}: H11), a ryanodine receptor-directed scorpion toxin identified within the venom of *Hadrurus gertschi*. Efficient internalization of QDs doubly functionalized with PEG5-CaRuby and H11 (in a molar ratio of 1:10:10, respectively) is demonstrated. In BHK cells expressing a *N*-methyl-D-aspartate receptor (NMDAR) construct, these nanobiosensors report rapid intracellular near-membrane Ca^{2+} transients following agonist application when imaged by TIRF microscopy. Our work presents the elaboration of cell-penetrating FRET-based nanobiosensors and validates their function for detection of intracellular Ca^{2+} transients.

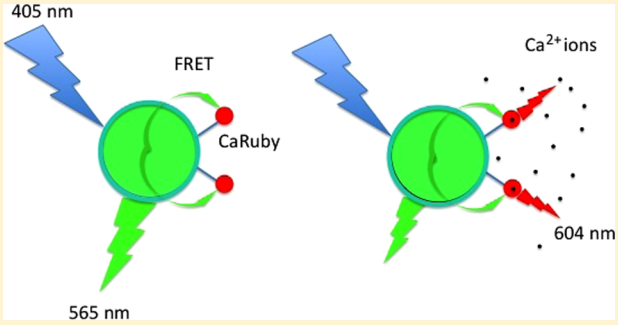

KEYWORDS: *Quantum dot biosensors, nanoparticle surface chemistry, FRET-based calcium probes, red-emitting calcium indicator, intracellular calcium fluorimetry, cell penetrating peptide*

Free calcium (Ca^{2+}) acts as a ubiquitous second messenger in numerous intracellular signaling pathways. Ca^{2+} controls cell metabolism, gene expression, vesicular trafficking and exocytosis to name a few functions. Ca^{2+} signals gain specificity by acting on different spatial and temporal scales. However, detecting fast and local Ca^{2+} concentration ($[Ca^{2+}]$) changes presents a major experimental challenge for microfluorimetric Ca^{2+} measurements with conventional Ca^{2+} indicators because only a few indicator molecules are localized in the small near-membrane volume invaded by local Ca^{2+} signaling events (see ref 1 for a measure of the external juxtacellular $[Ca^{2+}]$). Also, the intracellular diffusion of both the Ca^{2+} ions and the fluorescent Ca^{2+} indicator contributes to the rapid equilibration of Ca^{2+} gradients. Therefore, immobilizing and up-concentrat-

Received: November 12, 2013
Revised: April 16, 2014
Published: April 23, 2014

Table 1. Physical Parameters of QDs

QD donor	surface ligand	core/2 shells/surface ligand radius (nm)	QY %	ε^a (M^{-1} cm^{-1})	R_0 (Å) with CaRuby	r^e (Å) with PEG5 kDa
CANdot 565 organic	HDA/TOP/TOPO	~1.47[a] + 0.6[b] + ~1.2 = ~ 3.27	68	303764@405 nm 99040@543 nm		
CANdot 565-KC	50% pC/(pC + pK)	~1.8 ± 0.25[c]+	56	303764@405 nm	45	54
	85% pC/(pC + pK)	~2[d] = ~3.8	51	99040@543 nm		

[a]CdSe core estimated from the 543 nm first-exciton.[31] [b]CdS/ZnS shell.[32] [c]CdSe/CdS/ZnS by TEM (Supporting Information Figure S2). [d](pC+ pK) from ref 29 [e]See Figure 2b.

ing the Ca^{2+} sensitive dye, for example, by binding several molecules to a slowly diffusing dextran or nanoparticle is expected to report local [Ca^{2+}] transients more accurately.

The development of fluorescent inorganic colloidal nanoparticles (quantum dots, QDs, with a core diameter of 2−10 nm) that combine high brightness, photostability, and narrow emission spectra has been a breakthrough for single-particle imaging.[2,3] QDs are being used as molecular beacons to monitor enzymatic reactions,[2,4,5] track single vesicles following their endocytic uptake,[6] or for studying membrane diffusion of individual QD-tagged receptors,[6−9] all of which are experiments in which QDs report molecular position. Adding a sensing functionality to this localization information, for example, via Förster resonance energy transfer (FRET) opens new tracks for developing powerful tools in the fields of toxin detection, cell physiology, and pathology.[10−12]

Despite the synthesis and characterization of several nanobiosensors in vitro, their intracellular use is still challenging. Two major obstacles have impeded cell studies with FRET-based QD sensors: (i) in our experience, Ca^{2+} indicators that display low basal fluorescence and high sensitivity alone often show a disappointing performance once linked to a QD donor, and (ii) getting across the plasma membrane in a noninvasive way is another difficult step. Cationic liposomes yield generally low transfection rates while further inducing damaging cellular stress. The demonstration that ferromagnetic beads linked to Tat-derived cell penetrating peptides (CPPs) enter cells points to a potentially more efficient delivery strategy.[13] Besides penetratin, a peptide from the insect homeotic protein Antennapedia,[14,15] natural CPPs have been derived from scorpion toxins targeted toward the ryanodine receptor.[16−18] In contrast to the widely used positively charged CPPs,[19−21] these latter peptides efficiently drive internalization at nanomolar concentrations even if they are not charged.[22]

QDs functionalized with these peptides enter cells, the most potent ones delivering them into the cytoplasm rather than getting stuck in the endosomal pathway.[23,24] To date, no ionic nanobiosensor having both sensing and cell-penetrating function has been reported. The synthesis of such a nanobiosensor is complicated by the fact that QDs must be rendered water-soluble in a first step, bound to the Ca^{2+} indicator in a controlled manner (stoichiometry, donor/acceptor distance), and the CPPs linked to the surface as well.

Here, we design and validate both in vitro and in situ, a FRET-based cell-penetrating Ca^{2+} nanobiosensor combining a green fluorescent CdSe/CdS/ZnS (core/2 shells) QD donor with a red-fluorescent Ca^{2+} indicator of 3 μM affinity for Ca^{2+} binding (CaRubyMe).[25]

Our sensor is also functionalized with a H11 CPP from a scorpion toxin to facilitate its cytoplasmic entry. By building on the recently developed toolbox[25−27] of CaRuby Ca^{2+} indicators with affinities for Ca^{2+} binding ranging from 3 to 20 μM, Ca^{2+} biosensors with a similar architecture can be generated that will cover the entire biologically relevant range of local Ca^{2+} signals.

Results and Discussion. *Preparation of Hydrophilic Peptide-coated Quantum Dots.* We worked with a single, large batch of CANdots that combine high quantum yield (QY: 68%) and narrow peak emission at 565 ± 8 nm with a fwhm of 50 nm, that is, small size variability. With the first exciton peak at 543 nm, their emission overlaps with the absorption spectrum of our CaRubies (Supporting Information Figure S1), yielding a calculated Förster radius of 4.5 nm. We used a single batch, kept in hexane at 4 °C, that was stable over two years of experimentation.

To obtain hydrophilic QDs we used ligand exchange of the passivating trioctylphosphine/trioctylphosphine oxide (TOP/TOPO) layer by short phytochelatin-related peptides that bind by metal-affinity of a cysteine-rich $(FCC)_3$ adhesive domain to the CdZnSe QD surface.[28] The number of peptides that can be accommodated on a ~600 nm emitting QD is ~25−30 for the phytochelatin-like peptides[29,30] ensuring valence control. This amphiphilic peptide coating provides small diameter, monodisperse, negatively charged, hydrophilic nanoparticles with a high colloidal stability. Using transmission electron microscopy, we estimated their size and obtained a mean radius of 1.8 ± 0.25 nm (Supporting Information Figure S2). We showed that the average size of the core/2 shells particles remained the same while the total size of QDs slightly increased after the ligand exchange (Table 1).

To facilitate binding of biomolecules to the QDs we first introduced mixed SH-terminated and NH_2-terminated phytochelatin-like peptides (pC and pK, respectively, see legend of Figure 1 and Supporting Information Material and Methods) in a 1:1 ratio, half of them, the pCs, to be engaged in a SH/

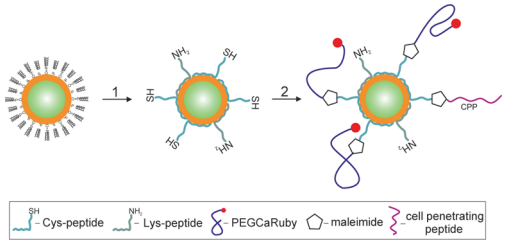

Figure 1. FRET-based Ca^{2+} biosensors. (Step 1) The QD TOP/TOPO passivating layer was replaced by a peptide coating made by mixing cysteine (SH function) and lysine (NH_2 function) terminated peptides (pC, Ac-CGSESGGSESG$(FCC)_3$F-amide; and pK, NH_2-KGSESGGSESG$(FCC)_3$F-amide respectively). Both components (hydrophobic QDs and peptides) were first dissolved in their respective solvents, pyridine and DMSO.[32] After mixing, surfactant exchange and peptide binding were initiated by raising the pH. (Step 2) Nanoparticles were further functionalized by adding CaRuby (red dots) and cell-penetrating peptides (CPP, purple wiggle) onto peptide-coated QDs using a SH/maleimide linking reaction.

dx.doi.org/10.1021/nl500733g | Nano Lett. 2014, 14, 2994−3001

maleimide linking reaction for further ligands conjugation[32] (Figure 1). The resulting constructs retained the photophysical properties of the original hydrophobic QDs (Table 1) with an only minor decrease of the fluorescence QY by ~12%. Because we aimed additionally at rendering the QDs membrane permeable by grafting CPPs, we considered increasing the relative number of pC peptides, but pC-only decorated QDs displayed a dramatically reduced QY. In contrast, by adding peptides in a 85:15% pC/pK ratio, some 25 SH sites are available for further conjugation[30] while keeping the QY at 51% (Table 1). We could thus investigate the properties of the FRET QDs-CaRuby pairs when varying acceptor to donor molar ratio (A/D).

Building of QD−CaRuby FRET pairs. CaRuby, the red-emitting Ca^{2+} indicator used here, is an extended rhodamine linked to a Ca^{2+}-chelating BAPTA moiety and having an additional linker arm (fluorescence excitation and emission peaks near 586 and 604 nm, respectively). Its Ca^{2+}-dependent fluorescence results from photoinduced electron transfer (PET) quenching. Ca^{2+} binding relieves PET and the fluorophore lights up.[26]

To functionalize QDs and avoid performing multiple reaction steps, we decided to synthesize a NH_2-terminated-PEG-CaRuby. The CaRuby PEGylation was efficiently performed with a commercially available NH_2-PEG-alkyne and CaRuby-N_3 by copper-catalyzed click chemistry. This compound was then transformed by a GMBS reaction into a maleimide-PEG-CaRuby for linkage. After binding maleimide-PEG-CaRuby to pC-sites of the QDs surface in a chosen QD/CaRuby stoichiometric ratio, the excess of unbound molecules of the dye was removed by dialysis (Supporting Information Figure S3).

Once assembled, we explored the spectral properties of the QD-CaRuby complexes in a 2 mM Ca^{2+} containing medium where FRET from the QD core to the rhodamine moiety is revealed. As illustrated in Figure 2 for QD-PEG5-CaRuby, FRET between the QD donor (D) and the CaRuby acceptor (A) increased with the number of CaRuby molecules, as expected for multiacceptor FRET.[33] We determined the A/D ratio by linear unmixing of the absorption spectra of the assembly using the pure A and D spectra. The A/D ratio was very close to the expected one, after correction for the fact that only 80% of the PEGs were labeled, implying an almost complete reaction. FRET efficiency ($E = 1 - F'_D/F_D$, where F'_D and F_D are the donor fluorescence intensities in the presence and absence of the acceptor, respectively) increased up to 80% while acceptor sensitization plateaued at 20% when the number of PEG5-CaRuby was increased up to 10. With a Förster radius of 4.5 nm, data of FRET efficiency (E) were well described by $E = nR_0^6/(nR_0^6 + r^6)$. Fit yielded a center-to-center distance r between donor and acceptor of 5.4 nm. This value results from the long 5 kDa PEG linker (black line in Figure 2b).

Ca^{2+} Sensing. Increasing the FRET efficiency should maximize the signal-to-noise ratio (SNR) for detecting Ca^{2+} transients. This can be achieved either by increasing A/D ratio (Figure 2a) or by reducing the D to A distance. To test the latter strategy, we prepared PEG-CaRubies of variable lengths: a custom-synthesized short <0.3 kDa NH_2-PEG-alkyne (see Supporting Information Materials and Methods, PEG0.3) and commercial 5 kDa (PEG5) and 10 kDa (PEG10) NH_2-PEG-alkyne. After coupling these CaRuby derivatives to the QDs, we systematically investigated the Ca^{2+}-sensitivity of the resulting FRET pairs with fluorimetric titrations in which we switched from a nominally Ca^{2+}-free solution (zero Ca^{2+} and 10 mM EGTA, peak photoluminescence, PL = F_0) to saturating (2 mM) Ca^{2+}: peak PL = F, and we used the relative increase in CaRuby fluorescence (dynamic range DR = $(F - F_0)/F_0$) as an index of sensitivity.

Although CaRuby retained a high Ca^{2+}-sensitivity after binding to PEG by click chemistry (DR = 60), unexpectedly, QD-CaRuby pairs built from short PEG0.3-CaRuby were largely Ca^{2+}-insensitive (DR = 0.5, n = 2). This was not due to the absence of FRET as evidenced by the donor quenching in the FRET pair (Figure 3b). Prasuhn et al.[34] obtained a Ca^{2+}-sensitive FRET signal when linking CaRuby to a QD through a short linker attached to a 6-His-terminated peptide composed of 2 α-helix turns. However, this signal was absent when a DHLA-PEG0.75 was intercalated instead of the peptide. This observation led us hypothesize that excessive proximity of the CaRuby to the QD surface perturbed Ca^{2+}-sensing. This should

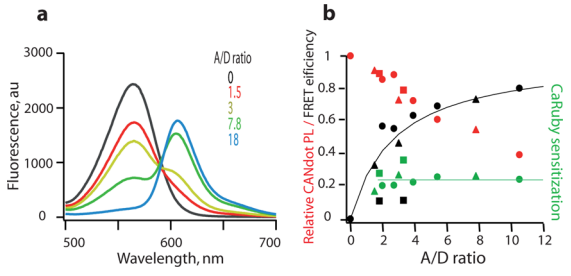

Figure 2. FRET upon 350 nm donor excitation, measured as donor quenching and acceptor sensitization, as a function of A/D ratio, at a constant [Ca^{2+}] of 2 mM. (a) Series of mixed spectra obtained by increasing the number of PEG5-CaRubyMe while keeping QD concentration constant. A/D ratio was measured by absorbance at 407 and 581 nm to evaluate QD and CaRuby concentrations, respectively. (b) Relative donor quenching (QD photoluminescence, red) and FRET efficiency (black) after linear unmixing. Acceptor sensitization (F_{CaRuby} (exc@350 nm) $-F_{QD}$ (exc@350 nm)/(F_{CaRuby} (exc@535 nm) is also reported (green). Symbols ▲, ●, ■ show results from 3 experiments; black line: fit with $E = nR_0^6/(nR_0^6 + r^6)$ with R_0 = 45.5 Å and variable r = 54.2 ± 1.6 Å. The line in green shows average acceptor sensitization for A/D ratio between 2 and 12 (~22%).

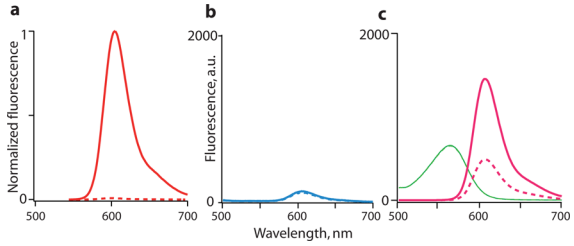

Figure 3. Emission spectra of FRET pairs in the presence (solid) and absence (dotted) of Ca^{2+}. (a) Normalized emission spectra of free PEG5-CaRuby. (b) Emission spectra of QD-PEG0.3-CaRuby with A/D = 18.8 (blue). (c) Spectra of QD-PEG5-CaRuby with A/D = 7.8. Acceptor and donor contribution to the spectra was separated by linear unmixing. FRET, estimated from QDs contribution to the spectrum, is unchanged (traces of QDs emission in 2 mM Ca^{2+} and 10 mM EGTA are superimposed). In panels b and c, QDs alone with no dye yielded a peak emission of about 2500 in both cases so allowing for direct comparison. In panel c, the same batch as in Figure 2 dark green trace.

dx.doi.org/10.1021/nl500733g | Nano Lett. 2014, 14, 2994−3001

not be the case when intercalating PEG5 or PEG10. However, even for these longer spacers the DR of the QD-CaRuby pair, while improving, remained quite low. At a 1:1 molar ratio, DR was ~1, as if CaRuby was still close to the QD surface, possibly due to the flexible PEG molecule backing upon itself. We therefore instead aimed at increasing the DR by systematically increasing the A/D ratio of PEG-CaRuby molecules bound onto a single QD, constructing stiffer "hairy ball" geometry.

Red fluorescence emission of QD-PEG5-CaRuby, either in response to direct excitation or via FRET, slowly but steadily increased with growing A/D ratio from 1 to 15 (Figure 4a; see

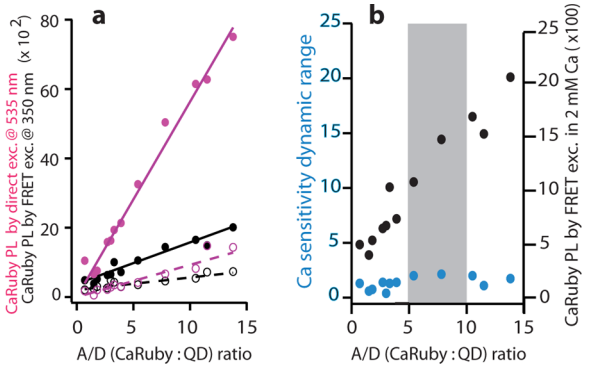

Figure 4. Ca^{2+} sensitivity of QD-PEG5-CaRuby as a function of A/D ratio. (a) CaRuby emission upon FRET excitation at 350 nm (in black) and direct excitation at 535 nm (in purple). Filled circles refer to measurements in a 2 mM Ca^{2+} and empty circles to measurements in 10 mM EGTA. FRET emission and PL obtained by direct excitation as well, linearly increase with an A/D ratio in the range 1−15 (PL by FRET in Ca^{2+} = 380 + 119 A/D ratio; FRET in EGTA = 200 + 36 A/D ratio). With CaRuby direct excitation, PL in Ca = 200 + 540 A/D ratio; in EGTA = 2 + 92 A/D ratio. (b) Summary graph displaying FRET absolute value increase (in 2 mM Ca^{2+}; black circles) whereas DR (blue dots) is constant when molar ratio was varied between 0 and 15. All data refer to the same QDs concentration. Data from 4 batches of QD-PEG5-CaRuby.

Supporting Information Figure S4 for QD-PEG10-CaRuby). In the same range, between 1 and 15 A/D, FRET efficiency (measured in 10 mM EGTA) also increased. As a result, the DR from the FRET-activated CaRuby was constant but low at ~2 (Figure 4b). With direct excitation, the DR was about twice as large but it never exceeded 5. Thus, while the DR of CaRuby is much reduced once linked to QDs, an A/D ratio in the range of 5−15 produces a Ca^{2+}-dependent fluorescence large enough to allow efficient Ca^{2+}-sensing (Figure 4b). As we aimed at visualizing and hence localize nanobiosensors inside the cell, even at resting intracellular $[Ca^{2+}]$, we finally retained an A/D ratio of 5−10 as a compromise for in situ experiments. Noticeably, these constructs proved to be stable over at least 2 months.

Next, we examined if the Ca^{2+}-binding affinity of CaRubyMe was changed by the nanosensor assembly. Samples of QD-PEG5-CaRubyMe (A/D ratio = 9) prepared at concentrations of 0.5 μM CaRuby were mixed with Ca^{2+} concentrations increasing from 0.1 up to 1000 μM (Figure 5a). Hill fit with fluorescence peaks from two separate experiments confirmed a K_d of 2.9 ± 0.3 μM (Figure 5b), not distinguishable from the 3.4 ± 0.5 μM, previously reported for CaRubyMe alone. Thus, despite its attachment in proximity of the highly charged QDs surface, CaRubyMe affinity for Ca^{2+} was unaltered. Furthermore, the k_{on} for Ca^{2+} binding to the nanobiosensors

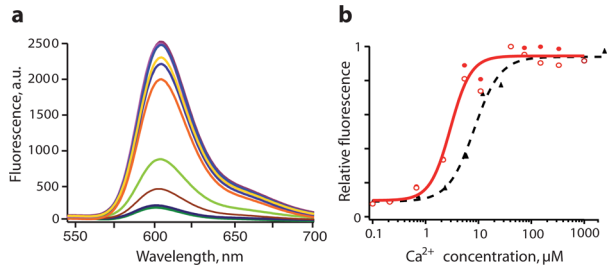

Figure 5. Fluorimetric titration against $[Ca^{2+}]$ of QD-PEG5-CaRubyMe complexes (A/D ratio = 9; buffer containing (in mM): 100 KCl and 30 MOPS, pH 7.2). (a) Superimposed fluorescence curves in the presence of increasing concentrations of Ca^{2+} as plotted in the dose−response curve on the right (red dots: direct excitation of CaRuby at 535 nm). (b) Peak fluorescence versus $[Ca^{2+}]$ for two independent titrations, filled and empty red dots, respectively. Red continuous line is Hill fit of all in cuvette data points, K_d = 2.9 ± 0.3 μM. Black triangles and dotted line show in cell-Ca2+ calibration using flow cytometry yielding a K_d of 7.6 ± 1.4 μM.

(calculated from the K_d and stopped-flow measurement of the k_{off}: ~150 s^{-1}) was of the order of 10^8 M^{-1} s^{-1}, as expected for BAPTA-based Ca^{2+} chelator.[35,36] This high k_{on} value makes our sensors an adequate tool for detecting fast $[Ca^{2+}]_i$ transients (Supporting Information Figure S5).

Internalization of Nanobiosensors. To promote the intracellular translocation of functionalized QDs, we used CPPs of specially high efficiency that we recently identified, derived from toxins targeted against the intracellular ryanodine receptor.[22] Uptake of H11 (Smartox Biotechnology, Saint Martin d'Hères, France), a CPP derived from the scorpion toxin hadrucalcin, was already significant at a concentration as low as 500 nM (Supporting Information Figure S6). Incubation of cells with 100 nM QDs functionalized with 5−10 CPPs brings CPP local concentration in this range. Baby hamster kidney cells (BHK-21) were incubated for 2 h with 100 nM QDs doubly functionalized with PEG5-CaRuby and H11 in the molar ratio 1:10:10 and the internalization efficiency was evaluated by live-cell confocal imaging. The nucleus and the plasma membrane were counterstained to better assess the cytoplasmic location of the QDs (Figure 6a).

As seen on the confocal section shown in Figure 6b, QD-CaRuby-H11 complexes penetrated inside the cells and were distributed throughout the cytoplasm. However, compared to conventional chemical Ca^{2+} indicators our sensors have a pointillistic distribution. This pointillistic distribution of our sensors provides a localized read-out of $[Ca^{2+}]$ at discrete points where the CaRuby has been up-concentrated. Internalization of functionalized QDs occurred without damaging side effects (Supporting Information Figure S7).

Because the number of internalized QDs varied from cell to cell, a first quantification of the internalized QDs was carried out using imaging flow cytometry. For the analysis QDs located in close vicinity to the plasma membrane were subtracted whether on its extracellular or intracellular sides. A number of QDs without CPPs were internalized; QDs internalization, however, as illustrated in Figure 6c, is almost doubled by CPPs addition, with no further improvement when going from 5 to 10 CPPs.

Electron micrographs of BHK cells loaded with QD-CaRuby-H11 complexes show groups of ~15−20 QDs dispersed over an area of ~500 nm diameter probably corresponding to the spots observed in confocal microscopy. Though at this point we

dx.doi.org/10.1021/nl500733g | Nano Lett. 2014, 14, 2994−3001

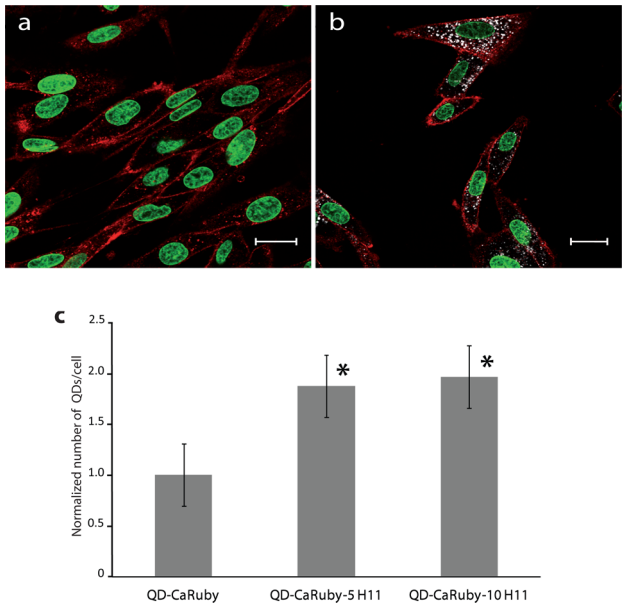

Figure 6. Cell penetration of QDs doubly functionalized with CaRuby and cell penetrating peptide H11. (a) Confocal microscopy section of live BHK-21 cells with Hoechst nuclear staining (green) and concanavalin-Alexa 647 membrane staining (red). (b) BHK-21 cells with internalized QDs. Gray dots show QDs-CaRuby-H11 emission upon direct excitation of CaRuby at 561 nm. Scale bar, 20 μm. (c) Imaging flow cytometry analysis of QDs penetration. Normalized average number of internalized QDs per cell for QD-CaRuby alone, QD-CaRuby-5H11, and QD-CaRuby-10H11 complexes, respectively. Measurements made upon CaRuby direct excitation at 561 nm. Data show mean ± s.e.m for 100 cells of each sample; *—p < 0,05 compared to QD-CaRuby.

do not know their exact path for cell entry, we show QDs to be not enclosed in a membrane-delimited compartment (Figure 7). This is the conclusion attained with a TEM image poorly contrasted to better see the small size QDs (Figure 7) and as well of an TEM image where the contrast has been increased to the point when some uranyl acetate deposits are formed (Supporting Information Figure S8). Thus, our nanobiosensors are exposed to the intracellular medium and hence should be able to report the local cytoplasmic Ca^{2+} concentration.

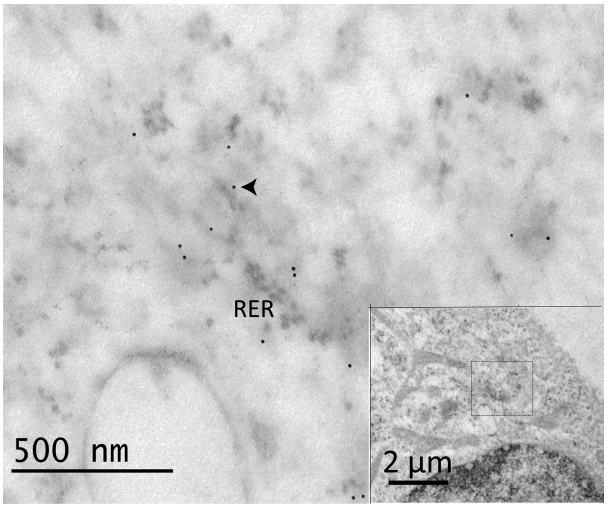

Figure 7. EM micrograph of QD-CaRuby-H11 complexes internalized in aBHK cell. Image shows zoom on the region of interest identified on the inset image. Individual QDs (arrow) appear as electron-dense spots of ~5 nm diameter, dispersed throughout the cytoplasm. Larger and less dense punctiform structures are the rough endoplasmic reticulum (RER) and ribosomes.

Intracellular Ca^{2+} Nanobiosensing. To demonstrate the Ca^{2+}-sensing ability of our sensors inside live cells we used HEK293 cells expressing *N*-methyl-D-aspartate receptors (NMDARs). These are plasma membrane cation-permeable channels mediating Ca^{2+} influx upon activation by agonist binding. Our nanobiosensors were loaded as described above, followed by the resuspension of the cells in a HEPES-buffered medium for time-lapse fluorescence measurements. External [Ca^{2+}] was raised to 10 mM to maximize Ca^{2+} entry upon receptors activation.

After loading of QD-CaRuby-H11 complexes, some QDs remained attached to the external side of plasma membrane, which resulted in a high background fluorescence. This background was efficiently reduced by adding to the extracellular saline 40 μM Cu^{2+}, an effective QDs and CaRuby quencher.[25,37] The Ca^{2+} binding affinity (K_d) to the nanosensor was slightly increased, an effect described for other Ca^{2+} indicators and possibly related to the higher viscosity of the intracellular medium (see Figure 5b dotted line).

Injection to the cell suspension of the NMDAR agonists glutamate and glycine in the presence of external Ca^{2+} produced an increase of the CaRuby fluorescence (Figure 8c, red trace), as expected from the NMDAR-mediated Ca^{2+} influx (Figure 8a), confirming the intracellular responsiveness of our Ca^{2+} nanobiosensors.

Preincubation of the cells with APV, a NMDAR antagonist, (Figure 8b) almost completely abolished the agonist-evoked

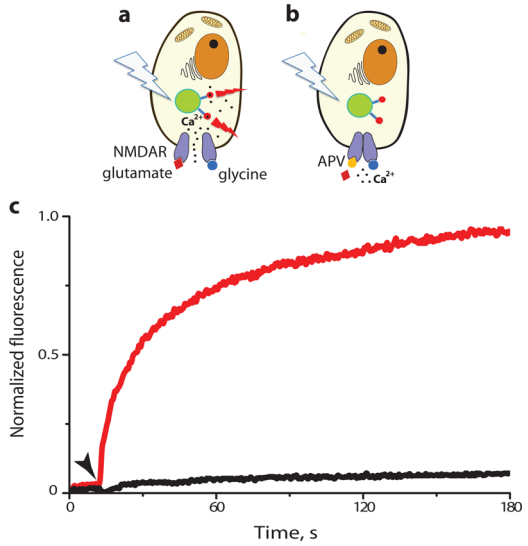

Figure 8. Intracellular [Ca^{2+}] measurement in a suspension of HEK293 cells transfected with NMDARs and incubated with 100 nM nanobiosensors. Schematic representation of (a) NMDAR activation by coapplication of agonists (100 μM glutamate and 20 μM glycine) followed by Ca^{2+} influx into the cell and (b) of the NMDAR blockade by an antagonist (100 μM APV) preventing Ca^{2+} influx upon application of the agonists. (c) Intracellular Ca^{2+}-dependent acceptor fluorescence as a function of time. Arrowhead marks application of agonists in absence of antagonist or after blocking NMDAR by APV, red and black traces, corresponding to conditions (a) and (b) respectively (2 replicates in 3 independent experiments).

dx.doi.org/10.1021/nl500733g | *Nano Lett.* 2014, 14, 2994−3001

Ca^{2+} response (Figure 8c, black trace). Likewise, no fluorescence increase was observed when applying agonists in Ca^{2+} free medium (data not shown). The Ca^{2+} response of our sensors is similar to that obtained using conventional dyes and cells, expressing the same subunits of NMDA receptor-channels.[38] We thus show that our QD-based Ca^{2+} nanobiosensors can specifically detect Ca^{2+} changes in a biologically relevant paradigm of receptor activation.

Finally, to demonstrate the ability of developed nanobiosensors to detect local subcellular Ca^{2+} signals in live cells, we loaded QD-CaRuby-H11 nanobiosensors into BHK cells stably expressing the NR1 and NR2 subunits of the NMDAR.[38] To visualize near-membrane QD sensors, we used total internal reflection fluorescence (TIRF) microscopy, simultaneously detecting in the green and red channel upon 405 and 568 nm evanescent-wave excitation on a custom prism-type VA TIRF microscope,[39] (Supporting Information Figure S9). To reduce noise caused by extracellularly attached QDs, QD-loaded cells were trypsinized and replated on quartz coverslips displaying a low autofluorescence. After trypsinization, transient $CuSO_4$ addition to BHK cells is not necessary unless an improved signal-to-noise ratio is sought (see Supporting Information Figure S10 illustrating the characteristics of the Cu^{2+} effect).

Evanescent-wave illumination allowed visualizing only those nanosensors close to the basal cell membrane with a high contrast, permitting readout of the fluorescence emitted by QD-sensors (Figure 9a,b). Ca^{2+} transients were evoked by NMDAR activation (100 μM glutamate, 20 μM glycine and 5 mM $CaCl_2$) and responses continuously recorded at 4 Hz during 3 min before and during agonists application. Figure 9c shows the Ca^{2+} transients detected at single sites, after background subtraction and correction for photobleaching, expressed as F/F_0, where F_0 is the (local) basal value before NMDAR activation. Our nanosensors read out local $[Ca^{2+}]$ transients that were distinct both, between cells (cell 1 and cell 2 in Figure 9c,d) and at the subcellular level, some displaying an F/F_0 up to 2.0 whereas some sensors nearby were silent and others show intermediary values.

Interestingly among the detected Ca^{2+} transients, the F/F_0 peak value read in a single cell at saturating concentration of agonists here applied was 2.2 ± 0.9 (ranging from 1.4 to 4.7, n = 14 cells, on 6 distinct coverslips from 4 distinct batches of cells). In cell 1, time constants at three regions of interest were 500, 700, and 900 ms, from top to bottom, respectively. In addition to variability in the agonist application, the distance from the biosensor to the Ca^{2+} source may account for such local variations. Along this line, the nonresponsiveness of red-emitting QDs is coherent with a localization in a cytoplasmic region ensuing no change in $[Ca^{2+}]$, but also alternatively with a localization in endosomes because this structure has a $[Ca^{2+}]$ saturating for the probe. Average kinetics of fluorescence transients recorded with QD-CaRuby-H11 were similar to those obtained with a conventional bulk-loaded small-molecule chemical Ca^{2+} indicator, X-rhod-1, AM, when the same cell was stimulated again following dye loading at the end of the experiment (Supporting Information Figure S10). Control applications in Ca^{2+}-free extracellular saline failed to produce measurable fluorescence changes.

Taken together, these experiments comfort our interpretation that QD-CaRuby-H11 sensors indeed detect cytoplasmic Ca^{2+} transients evoked by NMDAR-mediated Ca^{2+} influx across the plasma membrane. Furthermore, sequential applications of

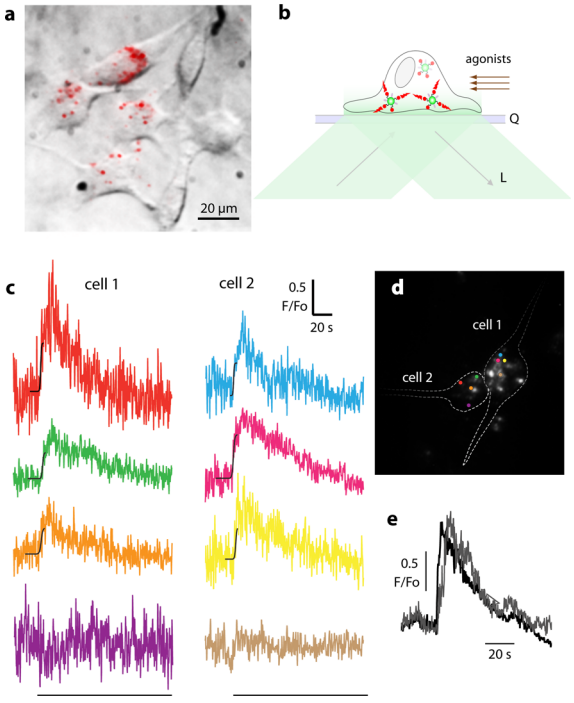

Figure 9. Read-out of local Ca^{2+} transients. (a) Localization of internalized biosensors (QD-CaRuby-H11 in a ratio 1:10:10) on the superimposed bright-field and time-averaged TIRF image of cultured BHK cells. (b) Schematic representation of the TIRF imaging of Ca^{2+} nanobiosensors. Confinement of excitation light (L) excites only fluorophores present in a ~100 nm layer above the quartz coverslip (Q). Among the three nanosensors schematized, only two are fluorescent while the third one is out-of-reach of the evanescent wave. (c) Local Ca^{2+} detection. Traces show simultaneously acquired transients in distinct spots in response to bath application of saturating concentrations of NMDAR agonists (during bottom black line) at various points in two neighboring cells "1" and "2" (left and right columns respectively); 700 images, t_{exp} = 250 ms. (d) Pseudocolor-overlay of spot positions on the cell outline. (e) Repetitive simulation evokes reversible Ca^{2+} transients. Superimposed traces, recorded at a same point, are responses to two successive bath applications of NMDAR agonists at a saturating concentration within between a 15 min long continuous bath perfusion of CTR saline for recovery from desensitization. Ca^{2+} signals were recorded with (c) and without (e) a previous transient application of Cu^{2+}.

NMADR agonists produced stereotyped reversible Ca^{2+} transients at the same site as expected (Figure 9e).

Compared to classical chemical Ca^{2+} indicators, FRET-based nanobiosensors are attractive for probing microdomain Ca^{2+} signals because, (i) QD-based, they combine high brightness with low cytoplasmic mobility[40−43] and low photobleaching compared to organic Ca^{2+} probes. (ii) They further allow localizing by green fluorescence candidate sites even at resting Ca^{2+}. (iii) With conventional chemical small-molecule Ca^{2+} indicators and genetically encoded Ca^{2+} indicators (GECIs), only a few indicator molecules are localized in the small near-membrane volume invaded by local Ca^{2+} signaling events.[44] Here, covalently linking the Ca^{2+} sensor to the QD surface locally up-concentrates the indicator up to the approximately millimolar range, a concentration that cannot be attained by simple aqueous dilution, thus (iv) permitting to attain signal-to-noise ratios favorable for the detection of fast and local Ca^{2+} transients. (v) Average cytoplasmic concentrations is maintained low, and hence exogenous Ca^{2+} buffer capacity. (vi)

dx.doi.org/10.1021/nl500733g | Nano Lett. 2014, 14, 2994−3001

Compared to other red-emitting low-affinity Ca^{2+} probes like Xrhod-5F or CaRuby-Cl alone, their large molecular weight prevents mitochondrial internalization and light-induced cytotoxicity.

Here, using a commercial QD donor, our CaRuby as a red-emitting Ca^{2+}-sensitive acceptor and a cell-penetrating peptide-derived cytoplasmically active toxin to facilitate cell entry, our Ca^{2+} nanobiosensors combine ease of synthesis, controlled stoichiometric assembly, high colloidal stability and efficient cytoplasmic delivery. Added to the extracellular saline, these Ca^{2+} nanobiosensors are internalized within 2 h to display a punctate cytoplasmic distribution when imaged with TIRF microscopy on the day thereafter, after replating. In a cell line stably expressing the Ca^{2+}-permeable NMDA receptor channel, we detected heterogeneous intracellular Ca^{2+} transients following receptor-activation with specific agonists, thus providing the first validation of Ca^{2+} nanobiosensors for subcellular biological Ca^{2+} imaging in live cells.

The next logical step is the targeting of our sensor by its further functionalization with specific antibodies to a high-conductivity Ca^{2+} channel such as the RyRs (400 pS) or NMDARs (50 pS) and perform optical single-channel recording.

■ ASSOCIATED CONTENT

Supporting Information

Eleven supplementary figures and their legends, detailed materials and methods, and abbreviations. This material is available free of charge via the Internet at http://pubs.acs.org.

■ AUTHOR INFORMATION

Corresponding Author

*E-mail: anne.feltz@ens.fr.

Present Addresses

(M.C.) UMR 7213 CNRS, Laboratoire de Biophotonique et Pharmacologie 74 route du Rhin, CS 60024, F - 67401 Illkirch 67400, France.

(A.V.Y) Biology Faculty, Kazan Federal University, Kazan, Russia

(A.I.Z., secondary address) Biomaterials and Nanomaterials Group, Department of Microbiology, Kazan Federal University, Kazan, Republic of Tatarstan, RF, 420008.

Author Contributions

The manuscript was written through contributions of all authors. All authors have given approval to the final version of the manuscript.

A.I.Z. and M.C. contributed equally to the work.

Notes

The authors declare no competing financial interest.

■ ACKNOWLEDGMENTS

We want to thank Institut Curie for giving us access to its Flow Cytometry platform, and especially to Mrs. Z. Maciorowski for her help in initiating us to this technique. O. Hernandez-Cubero helped us in the analysis of the TEM images. Christian Boudier (UMR7213 Laboratoire de Biophotonique et Pharmacologie, Strasbourg) a permis les expériences de "stopped flow". We thank Pierre Paoletti's group (IBENS, Paris) for providing the NMDAR (NR1 and NR2B) plasmids. We specially thank Dr. H. Bräuner-Osborne and J. Egebjerg (University of Copenhagen) for providing the BHK cell line stably expressing NR1 and NR2 subunits of the NMDA receptor that also proved to be strongly adherent to quartz coverslips making possible the present TIRF experiments. This work has received support under the program "Investissements d'Avenir" launched by the French government and implemented by the ANR (ANR-10-LABX-54 MEMO LIFE, ANR-11-IDEX-001-02-PSL). This work was supported by the French Agence National de la Recherche (ANR P3N, nanoFRET^2 grant, to A.F., J.M.M., M.d.W., M.O.) and the European Union (FP6 STRP AUTOSCREEN grant and FP7 ERA-NET NeuronNANOSYN grant to M.O.). M.O. is supported by the FranceBioImaging initiative (FBI).

■ REFERENCES

(1) Etter, E. F.; Kuhn, M. A.; Fay, F. S. *J. Biol. Chem.* **1994**, *269*, 10141−9.

(2) Alivisatos, A. P.; Gu, W.; Larabell, C. *Annu. Rev. Biomed Eng.* **2005**, *7*, 55−76.

(3) Michalet, X.; Pinaud, F. F.; Bentolila, L. A.; Tsay, J. M.; Doose, S.; Li, J. J.; Sundaresan, G.; Wu, A. M.; Gambhir, S. S.; Weiss, S. *Science* **2005**, *307*, 538−44.

(4) Biebricher, A.; Wende, W.; Escude, C.; Pingoud, A.; Desbiolles, P. *Biophys. J.* **2009**, *96*, L50−2.

(5) Lidke, D. S.; Nagy, P.; Heintzmann, R.; Arndt-Jovin, D. J.; Post, J. N.; Grecco, H. E.; Jares-Erijman, E. A.; Jovin, T. M. *Nat. Biotechnol.* **2004**, *22*, 198−203.

(6) Zhang, Q.; Li, Y.; Tsien, R. W. *Science* **2009**, *323*, 1448−53.

(7) Dahan, M.; Levi, S.; Luccardini, C.; Rostaing, P.; Riveau, B.; Triller, A. *Science* **2003**, *302*, 442−5.

(8) Saint-Michel, E.; Giannone, G.; Choquet, D.; Thoumine, O. *Biophys. J.* **2009**, *97*, 480−9.

(9) Triller, A.; Choquet, D. *Neuron* **2008**, *59*, 359−74.

(10) Delehanty, J. B.; Susumu, K.; Manthe, R. L.; Algar, W. R.; Medintz, I. L. *Anal. Chim. Acta* **2012**, *750*, 63−81.

(11) Sapsford, K. E.; Berti, L.; Medintz, I. L. *Angew. Chem., Int. Ed.* **2006**, *45*, 4562−89.

(12) Wang, Y.; Chen, L. *Nanomedicine* **2011**, *7*, 385−402.

(13) Josephson, L.; Tung, C. H.; Moore, A.; Weissleder, R. *Bioconjugate Chem.* **1999**, *10*, 186−191.

(14) Derossi, D.; Joliot, A. H.; Chassaing, G.; Prochiantz, A. *J. Biol. Chem.* **1994**, *269*, 10444−50.

(15) Joliot, A.; Pernelle, C.; Deagostini-Bazin, H.; Prochiantz, A. *Proc. Natl. Acad. Sci. U.S.A.* **1991**, *88*, 1864−8.

(16) Esteve, E.; Smida-Rezgui, S.; Sarkozi, S.; Szegedi, C.; Regaya, I.; Chen, L.; Altafaj, X.; Rochat, H.; Allen, P.; Pessah, I. N.; Marty, I.; Sabatier, J. M.; Jona, I.; De Waard, M.; Ronjat, M. *J. Biol. Chem.* **2003**, *278*, 37822−31.

(17) Poillot, C.; Bichraoui, H.; Tisseyre, C.; Bahembera, E.; Andreotti, N.; Sabatier, J. M.; Ronjat, M.; De Waard, M. *J. Biol. Chem.* **2012**, *287*, 17331−17342.

(18) Poillot, C.; Dridi, K.; Bichraoui, H.; Pecher, J.; Alphonse, S.; Douzi, B.; Ronjat, M.; Darbon, H.; De Waard, M. *J. Biol. Chem.* **2010**, *285*, 34168−80.

(19) Derossi, D.; Chassaing, G.; Prochiantz, A. *Trends Cell Biol.* **1998**, *8*, 84−7.

(20) Boeneman, K.; Delehanty, J. B.; Blanco-Canosa, J. B.; Susumu, K.; Stewart, M. H.; Oh, E.; Huston, A. L.; Dawson, G.; Ingale, S.; Walters, R.; Domowicz, M.; Deschamps, J. R.; Algar, W. R.; Dimaggio, S.; Manono, J.; Spillmann, C. M.; Thompson, D.; Jennings, T. L.; Dawson, P. E.; Medintz, I. L. *ACS Nano* **2013**, *7*, 3778−96.

(21) Walrant, A.; Vogel, A.; Correia, I.; Lequin, O.; Olausson, B. E.; Desbat, B.; Sagan, S.; Alves, I. D. *Biochim. Biophys. Acta* **2012**, *1818*, 1755−63.

(22) Tisseyre, C.; Bahembera, E.; Dardevet, L.; Sabatier, J. M.; Ronjat, M.; De Waard, M. *Pharmaceuticals* **2013**, *6*, 320−339.

(23) Ram, N.; Texier-Nogues, I.; Pernet-Gallay, K.; Poillot, C.; Ronjat, M.; Andrieux, A.; Arnoult, C.; Daou, J.; De Waard, M. *Int. J. Biomed. Nanosci. Nanotechnol.* **2011**, *2*, 12−32.

(24) Ram, N.; Weiss, N.; Texier-Nogues, I.; Aroui, S.; Andreotti, N.; Pirollet, F.; Ronjat, M.; Sabatier, J. M.; Darbon, H.; Jacquemond, V.; De Waard, M. *J. Biol. Chem.* **2008**, *283*, 27048−56.
(25) Collot, M.; Loukou, C.; Yakovlev, A. V.; Wilms, C. D.; Li, D.; Evrard, A.; Zamaleeva, A.; Bourdieu, L.; Leger, J. F.; Ropert, N.; Eilers, J.; Oheim, M.; Feltz, A.; Mallet, J. M. *J. Am. Chem. Soc.* **2012**, *134*, 14923−31.
(26) Gaillard, S.; Yakovlev, A.; Luccardini, C.; Oheim, M.; Feltz, A.; Mallet, J. M. *Org. Lett.* **2007**, *9*, 2629−32.
(27) Luccardini, C.; Yakovlev, A. V.; Pasche, M.; Gaillard, S.; Li, D.; Rousseau, F.; Ly, R.; Becherer, U.; Mallet, J. M.; Feltz, A.; Oheim, M. *Cell Calcium* **2009**, *45*, 275−83.
(28) Pinaud, F.; Michalet, X.; Bentolila, L. A.; Tsay, J. M.; Doose, S.; Li, J. J.; Iyer, G.; Weiss, S. *Biomaterials* **2006**, *27*, 1679−87.
(29) Clarke, S.; Pinaud, F.; Beutel, O.; You, C.; Piehler, J.; Dahan, M. *Nano Lett.* **2010**, *10*, 2147−54.
(30) Iyer, G.; Pinaud, F.; Tsay, J.; Weiss, S. *Small* **2007**, *3*, 793−8.
(31) Yu, W. W.; Qu, L.; Guo, W.; Peng, X. *Chem. Mater.* **2003**, *15*, 2854−2860.
(32) Pinaud, F.; King, D.; Moore, H. P.; Weiss, S. *J. Am. Chem. Soc.* **2004**, *126*, 6115−23.
(33) Yakovlev, A. V.; Zhang, F.; Zulqurnain, A.; Azhar-Zahoor, A.; Luccardini, C.; Gaillard, S.; Mallet, J. M.; Tauc, P.; Bro chon, J. C.; Parak, W. J.; Feltz, A.; Oheim, M. *Langmuir* **2009**, *25*, 3232−9.
(34) Prasuhn, D. E.; Feltz, A.; Blanco-Canosa, J. B.; Susumu, K.; Stewart, M. H.; Mei, B. C.; Yakovlev, A. V.; Loukov, C.; Mallet, J. M.; Oheim, M.; Dawson, P. E.; Medintz, I. L. *ACS Nano* **2010**, *4*, 5487−97.
(35) Kao, J. P.; Tsien, R. Y. *Biophys. J.* **1988**, *53*, 635−9.
(36) Jackson, A. P.; Timmerman, M. P.; Bagshaw, C. R.; Ashley, C. C. *FEBS Lett.* **1987**, *216*, 35−9.
(37) Xie, H.-Y.; Liang, J.-G.; Zhang, Z.-L.; Liu, Y.; He, Z.-K.; Pang, D.-W. *Spectrochim. Acta, Part A* **2004**, *60*, 2527−2530.
(38) Hansen, K. B.; Brauner-Osborne, H.; Egebjerg, J. *Comb Chem. High Throughput Screening* **2008**, *11*, 304−15.
(39) van't Hoff, M.; Reuter, M.; Dryden, D. T.; Oheim, M. *Phys. Chem. Chem. Phys.* **2009**, *11*, 7713−7720.
(40) Courty, S.; Luccardini, C.; Bellaiche, Y.; Cappello, G.; Dahan, M. *Nano Lett.* **2006**, *6*, 1491−5.
(41) Grünwald, D.; Hoekstra, A.; Dange, T.; Buschmann, V.; Kubitscheck, U. *ChemPhysChem* **2006**, *7*, 812−815.
(42) Yum, K.; Na, S.; Xiang, Y.; Wang, N.; Yu, M. F. *Nano Lett.* **2009**, *9*, 2193−2198.
(43) Delehanty, J. B.; Bradburne, C. E.; Susumu, K.; Boeneman, K.; Mei, B. C.; Farrell, D.; Blanco-Canosa, J. B.; Dawson, P. E.; Mattoussi, H.; Medintz, I. L. *J. Am. Chem. Soc.* **2011**, *133*, 10482−10489.
(44) Oheim, M.; van't Hoff, M.; Feltz, A.; Zamaleeva, A.; Mallet, J. M.; Collot, M. *Biochim. Biophys. Acta* **2014**.